FEBS Letters

The helical propensity of the extracellular loop is responsible for the substrate specificity of Fe(III)-phytosiderophore transporters

Erisa Harada[1], Kenji Sugase[1,†], Kosuke Namba[2] and Yoshiko Murata[1]

1 Bioorganic Research Institute, Suntory Foundation for Life Sciences, Kyoto, Japan
2 Department of Pharmaceutical Science, Tokushima University, Japan

Correspondence
Y. Murata, Bioorganic Research Institute, Suntory Foundation for Life Sciences, 8-1-1 Seikadai, Seika-cho, Soraku-gun, Kyoto 619-0284, Japan
Fax: +81 774 98 6292
Tel: +81 50 3182 0705
E-mail: murata@sunbor.or.jp

Present address
†Department of Molecular Engineering, Graduate School of Engineering, Kyoto University, Kyoto, Japan

(Received 8 June 2016, revised 30 October 2016, accepted 3 November 2016, available online 23 November 2016)

doi:10.1002/1873-3468.12482

Edited by Julian Schroeder

***Hordeum vulgare* L. yellow stripe 1 (HvYS1) is a selective transporter of Fe (III)-phytosiderophores in barley that is responsible for iron acquisition from the soil. In contrast, maize *Zea mays*, yellow stripe 1 (ZmYS1) possesses broad substrate specificity. In this study, a quantitative evaluation of the transport activities of HvYS1 and ZmYS1 chimera proteins revealed that the seventh extracellular membrane loop is essential for substrate specificity. The loop peptides of both transporters were prepared and analysed by circular dichroism and NMR. The spectra revealed a higher propensity for α-helical conformation of the HvYS1 loop peptide and a largely disordered structure for that of ZmYS1. These structural differences are potentially responsible for the substrate specificities of the transporters.**

Keywords: α-helical content; phytosiderophore; YS1 transporter

Iron (Fe) is an element essential to life in all organisms from microbes to the animal kingdom. As humans heavily depend on plants for dietary purposes, iron acquisition from plants is important to our nutrition [1,2]. However, Fe forms insoluble ferric (Fe(III)) complexes in neutral and alkaline soils, which generally prevent the effective uptake of Fe into the roots [3,4]. Plants of the Poaceae family efficiently acquire insoluble Fe(III) by secreting iron-chelating phytosiderophores (PS) such as mugineic acids (MAs) [3–7]. The chelated iron is absorbed as soluble complexes by the roots via transporting proteins. In maize (*Zea mays*), yellow stripe 1 (ZmYS1) was identified as an iron-chelating PS transporter in the roots [8]. We have previously reported that the biological relevance of 2′-deoxymugineic acid (DMA, one of the MA analogues) not only acts as an Fe chelator but also as a trigger for the restoration of nitrate assimilation for coordinated growth under high pH conditions [9]. Upon absorption by the root, Fe is translocated to the shoots through the xylem as Fe(III)-citrate [10], while Fe(II)-nicotianamine (NA, a precursor of MA) moves in the phloem for long-distance transport, particularly in higher plants [11–13].

We have reported that *Hordeum vulgare* L. yellow stripe 1 (HvYS1) is a selective transporter for Fe(III)-PS, which is specifically expressed in the root epidermal cells [14]. In contrast, despite its high sequence homology with HvYS1 [14], maize ZmYS1 possesses

Abbreviations
CD, circular dichroism; DMA, 2′-deoxymugineic acid; DPC, dodecylphosphocholine; GB1, protein G B1 domain; MA, mugineic acid; NA, nicotianamine; PS, phytosiderophore; YS1, yellow stripe 1; YSL, yellow stripe 1-like.

considerable substrate promiscuity, transporting metal-MA complexes such as Cd(II)-, Co(II)-, Cu(II)-, Fe(II)-, Mn(II)-, Ni(II)-, Zn(II)-MAs and NA complexed with Fe(II) and Ni(II) in addition to Fe(III)-MAs [15–17]. Membrane trafficking of MA- or NA-metal complexes is mediated by YS1 and yellow stripe 1-like (YSL) transporter proteins, the latter of which are members of the YSL family; both of them play an important role in plant metal homeostasis [11,15]. Despite the high homology among the YS1/YSL family proteins, many of their members, such as HvYSL2 and HvYSL5, possess different substrate specificities; HvYSL2 is localized in the endodermis of roots and transports PS complexed with Fe(III), Zn(II), Ni(II), Cu(II), Mn(II) and Co(II) [18], whereas HvYSL5 occurs in all root cells and has an unknown substrate [19]. Eighteen *YSL* genes have been identified in rice (*Oryza sativa* L.) [15]. OsYSL15 is closely related to ZmYS1 and transports Fe(III)-DMA [20,21]. Recently, the model grass *Brachypodium distachyon* has been shown to express nineteen YS1 orthologues, such as BdYS1A and BdYS1B [22]. However, BdYS1A transports Fe(III)-DMA while BdYS1B lacks this activity [22]. The distinct differences in substrate recognition among the YS1/YSL family transporters motivated us to investigate the mechanism underlying their specificities.

We have previously reported that HvYS1 is the closest homologue to ZmYS1, with a sequence similarity of 95.0% [14], but the N-terminal outer membrane region (residues 1–50 of HvYS1 and 1–53 of ZmYS1) and the seventh extracellular loop (residues 353–392 of HvYS1 and 356–397 of ZmYS1) exhibit relatively low sequence similarities (30.6% and 32.5% respectively). We showed that the loop is responsible for the Fe(III)-PS specificity of HvYS1 based on an extensive assessment of transport activity for a series of HvYS1-ZmYS1 chimeras. The chimeras were constructed by exchanging the N-terminal regions (residues 1–313 of HvYS1 and 1–316 of ZmYS1), C-terminal regions (residues 386–678 of HvYS1 and 390–682 of ZmYS1), or central regions (residues 314–385 of HvYS1 and 317–389 of ZmYS1) of the proteins using conserved *Kpn*I and *Bgl*II cloning sites [23]. The two cloning sites are located close to either ends of the extracellular membrane loop; therefore, the central regions include the transmembrane region and some flanking residues of the loop. Circular dichroism (CD) analysis indicated that a synthetic 20-mer peptide corresponding to a portion of the extracellular membrane loop of HvYS1 forms an α-helix in solution, but the corresponding region in ZmYS1 is disordered [23].

In this study, we specifically identified the region responsible for the substrate specificity of HvYS1 in the previously determined extracellular membrane loop by exchanging the exact central regions (residues 350–392 of HvYS1 and 353–396 of ZmYS1) of the seventh extracellular membrane loop. Detailed electrophysiological analyses of transporter activity for the newly constructed chimeras in oocytes, including their transportation kinetic parameters, showed that this loop is essential for the substrate specificity of HvYS1. NMR and CD spectra of the peptides corresponding to the loop regions of HvYS1 (41 residues) and ZmYS1 (42 residues) revealed that this loop peptide forms an α-helix in HvYS1, whereas it shows a random coil structure in ZmYS1.

Materials and methods

Electrophysiological studies in *Xenopus laevis* oocytes

HvYS1-ZmYS1 chimeric transporters were constructed by exchanging the extracellular loop regions of HvYS1 (residues 350–392) and ZmYS1 (residues 353–396), designated 'Hv-Zm-Hv' and 'Zm-Hv-Zm'. The Hv-Zm-Hv chimeric construct was prepared by the megaprimer PCR method (first PCR primers: forward, TACCACTTCATAAAAATTGTT GGTGTCACTGTT; reverse, CCATCCAAGAGGGGAAA GACCCGTCGCTG; second PCR primers: forward, TACC ACTTCATAAAAATTGTTGGTGTCACTGTTAAGAG; reverse, ACAAGGCATAACCAGCGTATGCCATCCAA GAGGGGA) using the QuikChange II site-directed mutagenesis kit (Agilent Technology, Santa Clara, CA, USA) and a HvYS1/pSP64 poly(A) *X. laevis* oocyte expression vector (Promega, Madison, WI, USA). The Zm-Hv-Zm chimeric construct was prepared using the ZmYS1/pSP64 vector by the megaprimer PCR (first PCR primers: forward, TCTGCATAGCTCTGATCATGGGAGACGGTACATA CCA; reverse, GGCGTACCCGGCGTAAGCTGCCCAG GC) and overlap extension PCR (first PCR primers: forward, CCTGGACAAGAAGACGTACGAG; reverse, M13R; second PCR primers: forward, CCTGGACAAGAA GACGTACGAG; reverse, TTCACCTTCTCCCAGACA) methods. The PCR products were inserted into ZmYS1/pSP64 poly(A) vector at the *Kpn*I and *Bam*HI sites. *Bam*HI was used to linearize HvYS1, ZmYS1, Hv-Zm-Hv, and Zm-Hv-Zm/pSP64 vectors, and cRNA transcription was performed *in vitro* with the SP6 mMESSAGE mMACHINE kit (Ambion, Austin, TX, USA). The cRNA solutions (0.1 $\mu g \cdot \mu L^{-1}$; 50 nL) were injected into oocytes and incubated in ND96 buffer (pH 7.6) for 3 days at 16 °C. Oocytes injected with water served as a negative control. The oocytes were voltage-clamped at −60 mV with an OC-725C oocyte clamp (Warner Instruments, Hamden, CT, USA) and steady-state currents were obtained after the addition of the Fe(III)-DMA or Fe(II)-NA complex (10 μL of 0.5, 2.5, 5, 10 and 20 mM for final

concentrations of 5, 25, 50, 100 and 200 μM respectively). DMA was chemically synthesized as described previously [24] and NA was purchased from T. Hasegawa Co., Ltd. (Tokyo, Japan). Fe(III)-DMA and Fe(II)-NA complexes were prepared as described previously [9,14,17]. To prepare Fe(III)-DMA, 500 mM DMA solution was mixed with 50 mM $FeCl_3$ in 10 mM MES/Tris Buffer (pH 7.6). To prepare Fe(II)-NA, 200 mM NA (incubated at 65 °C for 10 min) was mixed with 50 mM $FeSO_4$ in 10 mM MES/Tris Buffer (pH 7.6) containing 1 mM sodium ascorbate (Sigma-Aldrich, St. Louis, MO, USA) for 2 h in the dark. Both Fe(III)-DMA and Fe(II)-NA solutions were filtered using Ultrafree-MC Centrifugal Filter Devices (Merck Millipore, Billerica, MA, USA) by centrifugation at 13 000 ***g*** for 10 min at room temperature. Acquisition and all subsequent analyses were performed using p-Clamp 10 (Molecular Devices, Sunnyvale, CA, USA).

Preparation of HvYS1 and ZmYS1 loop fragments

The DNA sequence coding for the extracellular loop region of HvYS1 (residues 350–392) or ZmYS1 (residues 353–396) and the gene encoding the protein G B1 domain (GB1) with a hexahistidine tag were inserted into the pET21a vector at the restriction enzyme sites *Arv*II and *Bam*HI [25]. By modifying the *Arv*II site to introduce a factor Xa cleavage site, GB1 fusion HvYS1 (residues 352–392) and ZmYS1 (residues 355–396) constructs were created. All constructs were propagated in the *Escherichia coli* strain BL21 (DE3). GB1 fusion peptides labelled with $^{13}C/^{15}N$ were prepared by growing cells in minimum M9 medium supplemented with ^{15}N ammonium chloride, ^{15}N ammonium sulphate, and $^{13}C_6$ glucose (as sources of nitrogen and carbon respectively). GB1 fusion peptide expression was induced by adding 0.8−1.0 mM isopropyl β-$_D$-thiogalactopyranoside. The cells were further grown at 287 K for 48−50 h postinduction. After centrifugation, the harvested cells were suspended in 20 mM Tris-HCl (pH 7.6). The GB1 fusion peptides accumulated in the supernatant fraction were purified by C8 reverse-phase high-performance liquid chromatography (HPLC; Waters, Milford, MA, USA) using a water/acetonitrile gradient containing 0.1% trifluoroacetic acid. The purified GB1 fusion peptides were digested with factor Xa (New England Biolabs, Ipswich, MA, USA) in buffer containing 20 mM Tris-HCl (pH 7.4), 200 mM NaCl and 2 mM $CaCl_2$. The digested peptides were finally purified by HPLC. The molecular weights of the purified peptides were confirmed by Ultraflex III matrix-assisted laser desorption/ionization-time of flight-mass spectrometry (MALDI-TOF-MS; Bruker Daltonics, Bremen, Germany) and by using an Orbitrap Elite hybrid mass spectrometer (Thermo Fisher Scientific, Waltham, MA, USA). The peptide concentrations were determined by a standard BCA assay (Thermo Scientific Pierce, Rockford, IL, USA).

CD spectroscopy

Circular dichroism experiments were performed using a J-725 spectrophotometer (JASCO, Tokyo, Japan) with a 0.5-mm cell in 10 mM Tris-HCl (pH 7.0) buffer at 298 K. The CD spectra were measured at peptide concentrations of 0.23–0.28 $mg{\cdot}mL^{-1}$, with and without membrane-mimicking dodecylphosphocholine (DPC) micelles. The peptide/micelle ratio was 1 : 100. The secondary structures were estimated from the CD spectra using the CDPRO program [26,27].

NMR spectroscopy

Nuclear magnetic resonance samples contained ~ 0.5 mM $^{13}C/^{15}N$-labelled HvYS1 or ZmYS1 loop fragment in 20 mM Tris-HCl and 50 mM NaCl buffer (pH 7.0) prepared with 95% H_2O/5% D_2O. Standard three-dimensional NMR measurements (HNCO, HNCACO, HNCACB, CBCA(CO)NH and CC(CO)NH) [28–33] were performed using an AVANCE DMX750 spectrometer (Bruker BioSpin AG, Fällanden, Switzerland) equipped with a 5-mm cryogenic TXI probe at 298 K. Transverse relaxation-optimized spectroscopy-type three-dimensional measurements [34] were performed for the HvYS1 loop fragment with a 100-fold molar excess of deuterated DPC micelles. NMR data were processed using the NMRPIPE program [35], and the backbone chemical shift assignments were performed using the KUJIRA [36] and MAGRO programs [37]. The secondary structures were predicted from the obtained ^{13}C and ^{15}N chemical shifts using the TALOS+ program [38].

Results and Discussion

Activities of chimeric transporters

We have previously assigned the transmembrane regions of HvYS1 in comparison to those of ZmYS1 using the SOSUI program [39]. However, in a recent review comparing the topology prediction capacity of SOSUI and the TOPCONS program [40] TOPCONS identified fifteen transmembrane regions in ZmYS1 [15]. In this study, the transmembrane topologies of HvYS1 and ZmYS1 including Fe(III)-MAs transporters were re-examined with TMHMM [41] (Table S1 and Fig. S1); in contrast to previous predictions, we predicted that both HvYS1 and ZmYS1 expressed the focused loop fragments on the extracellular side [23]. The transmembrane regions of HvYS1 and ZmYS1 predicted by TMHMM are marked with blue lines in Fig. 1. The HvYS1-ZmYS1 chimeras were prepared by exchanging the predicted extracellular loop regions between the seventh and eighth transmembrane helices of the HvYS1 or ZmYS1 protein (Fig. 1).

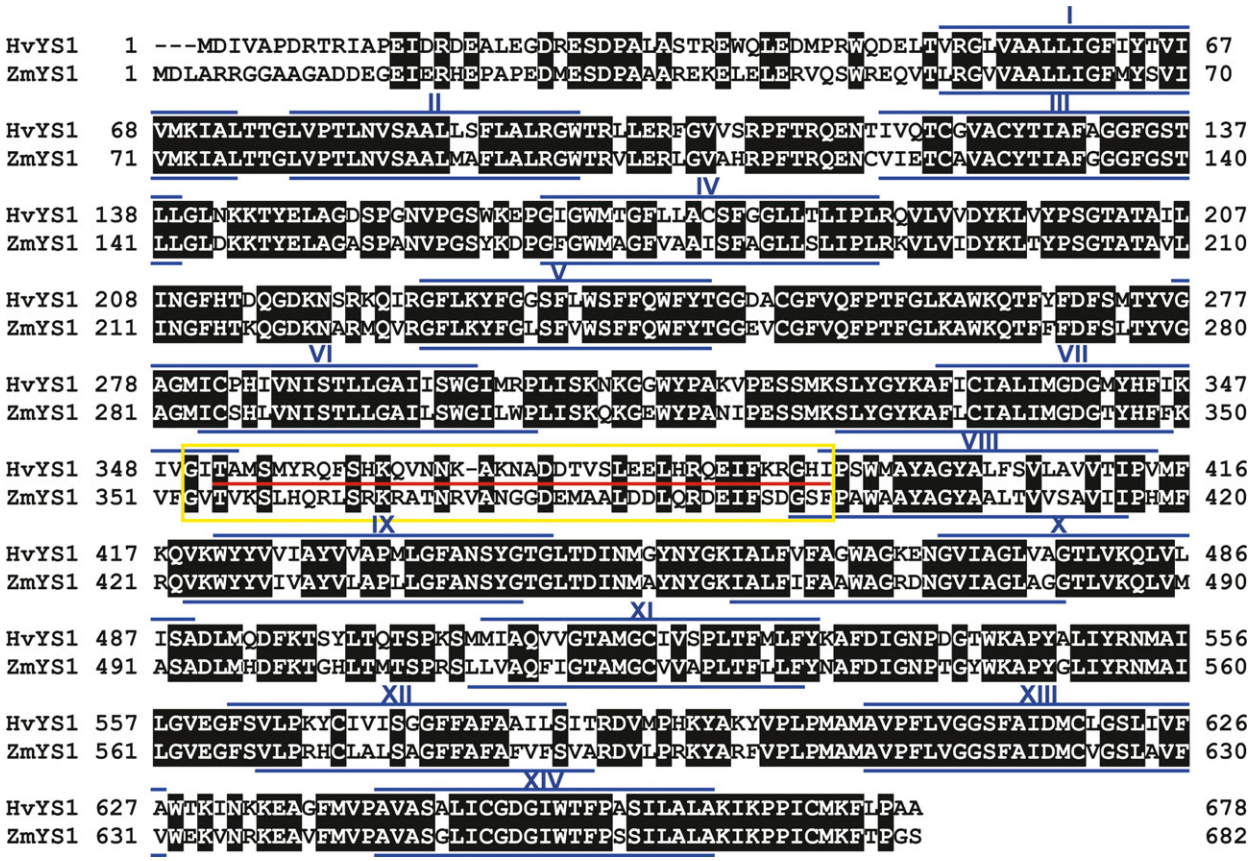

Fig. 1. Comparison of amino acid sequences of HvYS1 and ZmYS1. The 14 transmembrane regions of HvYS1 and ZmYS1 predicted by TMHMM are indicated with blue lines. The yellow box depicts the exchanged region in the HvYS1-ZmYS1 chimeras for the measurement of transport activity (Fig. 2). The loop fragments subjected to CD and NMR analyses are indicated with a red line.

Together with HvYS1 and ZmYS1, the chimeric proteins Hv-Zm-Hv and Zm-Hv-Zm (yellow box in Fig. 1) were heterologously expressed in *X. laevis* oocytes. To measure currents through the expressed transporters, the oocytes were voltage-clamped at −60 mV and superfused with buffer (pH 7.6) containing 0.5, 25, 50, 100 or 200 μM Fe(III)-DMA (Fig. 2A, B) or Fe(II)-NA (Fig. 2C,D). No currents were detected in water-injected control oocytes (data not shown). As shown in Fig. 2A,B, all proteins exhibited similar transport activities for Fe(III)-DMA, that is, HvYS1 (K_m = 71.8 μM), ZmYS1 (K_m = 65.3 μM), Hv-Zm-Hv (K_m = 60.8 μM) and Zm-Hv-Zm (K_m = 44.2 μM). The comparable results for the chimeric and wild-type proteins revealed the stability of their enzymatic activities under the experimental conditions (Fig. S2). The K_m of 65.3 μM for ZmYS1 in this study is higher than that of 5–10 μM reported before [17]. Small differences in experimental conditions including pH (pH 7.6 in this study and pH 6.0 in the previous one) may influence the difference in K_m values. We used ND96 buffer at pH 7.6 for oocyte experiments because this buffer and pH are suitable for maintaining the quality of *X. laevis* oocytes.

For Fe(II)-NA transport, however, the activities of HvYS1 and Zm-Hv-Zm were significantly lower than those of Hv-Zm-Hv and ZmYS1 (Fig. 2C,D), although K_m values for the Fe(II)-NA complex could not be determined due to a short supply of NA. These results demonstrated that the extracellular loop between the seventh and eighth transmembrane regions of the HvYS1 protein is responsible for its higher selectivity for Fe(III)-DMA than for Fe(II)-NA.

α-Helix prediction and measurement of CD spectra

Circular dichroism spectra were examined to estimate the secondary structures of the loop fragments in aqueous and membrane-mimicking solutions. The

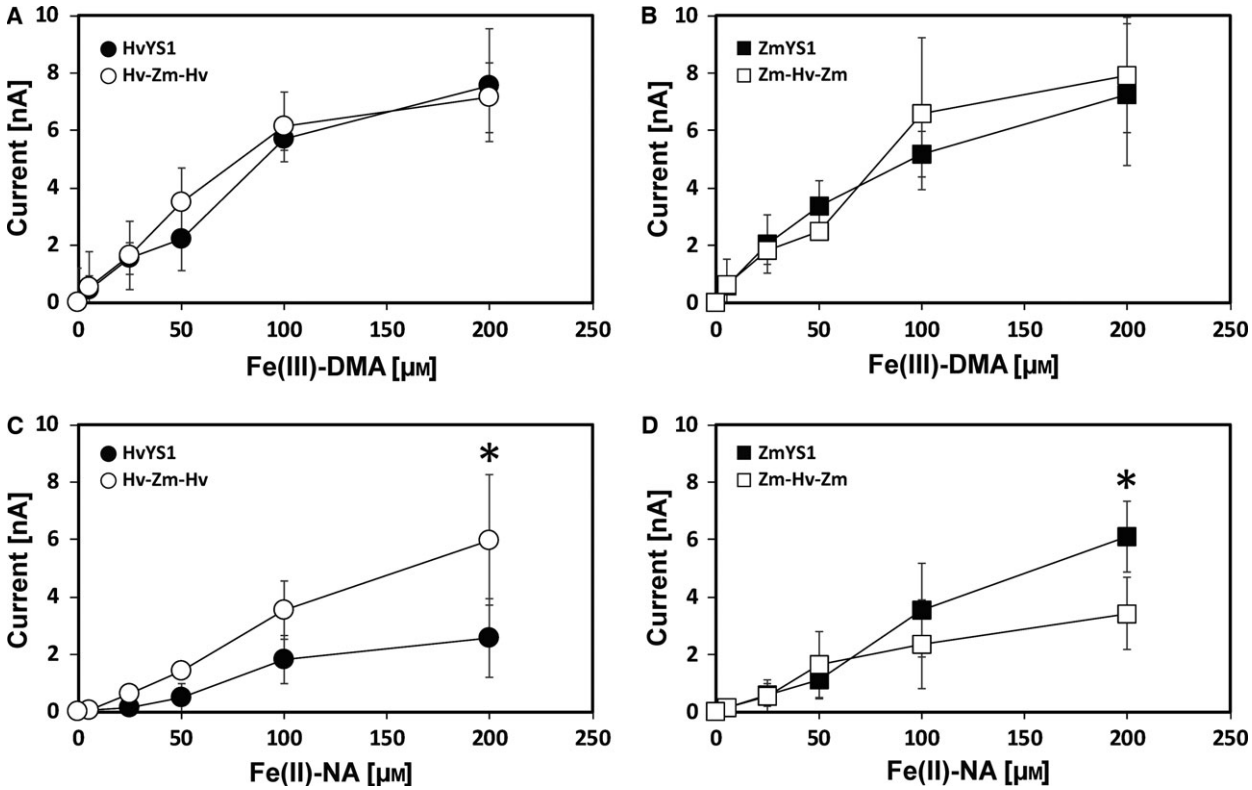

Fig. 2. Transport activities of HvYS1, ZmYS1, and the chimeras. PS concentration-dependent activities of wild-type HvYS1 (black circle) and chimeric Hv-Zm-Hv (open circle) (A, C) and ZmYS1 (black square) and Zm-Hv-Zm (open square) (B, D), which were obtained by exchanging the extracellular loop regions of HvYS1 (residues 350–392) and ZmYS1 (residues 353–396). These proteins were subjected to current measurements using a two-electrode voltage clamp method with *Xenopus laevis* oocytes. The transport activities for Fe(III)-DMA (A, B) and Fe(II)-NA (C, D) are shown. Experiments were repeated using 3–6 oocytes. Error bars show standard errors of the mean. $*P < 0.05$.

HvYS1 and ZmYS1 transporters exert their effects on substrate export through the membrane. Therefore, the membrane environment is important for maintenance of their native structures. A number of biophysical studies on peptides and proteins corresponding to the natural sequences of loops and cytoplasmic domains such as the G-protein-coupled receptors and viral proteins demonstrate that these protein fragments exhibit different degrees of helicity in aqueous versus membrane-mimicking environments [42,43]. Zwitterionic DPC micelles are frequently used as membrane mimics because the phosphatidylcholine headgroup of DPC is similar to those involved in protein–lipid interactions in eukaryote membranes. The CD spectra of the loop fragments of HvYS1 and ZmYS1 in the absence and presence of membrane-mimicking DPC micelles are shown in Fig. 3. The HvYS1 loop fragment possessed 16.9% helical content, whereas the ZmYS1 loop fragment mostly showed a random coil structure; the intensity of the negative band at 222 nm – marked with an asterisk in Fig. 3 – indicates α-helical content. The addition of DPC micelles altered the CD spectrum of the HvYS1 loop fragment slightly owing to an increase in the helical content to 31.8%. In contrast, the secondary structure of the ZmYS1 loop fragment remained largely unchanged (from 1.9% to 3.1%).

NMR study of HvYS1 and ZmYS1 loop fragments

The HvYS1 and ZmYS1 loop fragments were analysed by NMR to obtain residue-specific structural information. As seen in the CD spectra, the heteronuclear single quantum coherence (HSQC) spectra of both loop fragments showed narrow chemical shift dispersion in the ^{1}H dimension, corresponding to random coil chemical shifts (Fig. 4A). Compared to the HvYS1 loop fragment, the ZmYS1 loop fragment presented a poorly resolved spectrum (Fig. 4A). $^{1}H^{N}$ and ^{15}N backbone signals were assigned to 35 (out of 41) residues in the HvYS1 loop fragments and 36 (out of 42) residues in the ZmYS1 loop fragments. Residues to

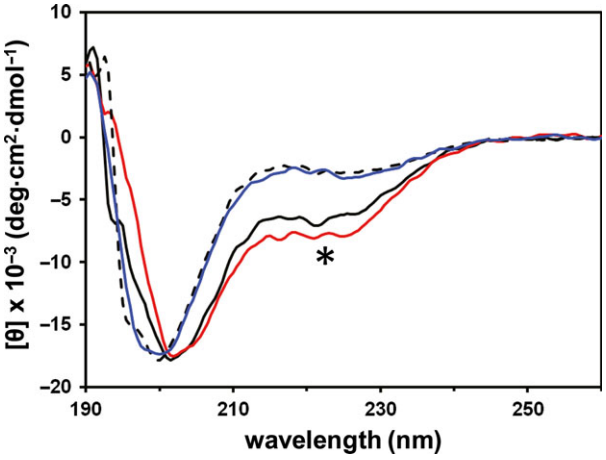

Fig. 3. CD spectra of the HvYS1 and ZmYS1 loop fragments. The HvYS1 loop fragments in buffer without and with membrane-mimicking DPC micelles are shown in black and red respectively. The ZmYS1 loop fragment in buffer without and with membrane-mimicking DPC micelles are denoted by a black dotted and blue line respectively. *Negative bands at 222 nm correspond to the α-helical content of each peptide.

which backbone signals were not assigned were located near the N-terminus of both loop fragments. The secondary structures were predicted by TALOS+ using the obtained chemical shift assignments. We confirmed that residues L378–F387 of the HvYS1 loop fragment form a helical structure, whereas the corresponding loop fragment of ZmYS1 showed a random structure (Fig. 5A,B). Residues E379, E380, H382 and Q384 in the α-helical structural region of HvYS1 were not conserved between HvYS1 and ZmYS1 (Fig. 1), suggesting that these residues are responsible for the formation of helical structures.

Because the CD spectrum of the HvYS1 fragment was changed by the addition of DPC micelles, the HvYS1 loop fragment was analysed by NMR under the addition of the micelles (Fig. 4B,C). Induced chemical shift changes were observed in the regions close to the N- and C-termini of the fragment. In particular, M354–F360 of the N-terminal region, where the unstructured secondary structure was converted to an α-helical structure, showed large chemical shift changes upon the addition of DPC micelles (Fig. 5C). The chemical shift analysis indicated that 24% (10/41) and 41% (17/41) of the amino acid residues in the HvYS1 loop fragment formed an α-helical structure in the absence and presence of DPC micelles respectively. This DPC-elicited increase in helical content of the HvYS1 loop fragment is in agreement with the CD results.

The loop fragment of HvYS1 showed a helical structure at the N-terminus under the membrane-mimicking conditions and the loop region of the transporter was most likely anchored to the membrane surface by neighbouring transmembrane helices. Therefore, the corresponding loop of HvYS1 could be more stable in the membrane environment than in the buffer, which beneficially modulates the transporter function [43,44]. Indeed, the transport activities of the chimeric proteins did not differ from those of wild-type proteins, suggesting that the exchanged loop region mainly contributed to the selectivity of the transporters towards metal-PS complexes. HvYS1 is predicted to possess the highest helical content (29.2% α-helical content) in the homologous loop region among proteins in the YS1/YSL family (Table S1). HvYSL2, an HvYS1 homologue with broad substrate specificity [18], has low α-helix content (2.5%) in the loop region, similar to ZmYS1 (4.1%) and other YSL transporters with 1.9–5.1% α-helices in the corresponding loop as predicted by AGADIR [23]. Therefore, we assumed that the markedly high helical propensity of HvYS1 in the loop region and/or the helical structure induced in the membrane environment acts as a filter for metal-PS complexes to select Fe(III)-DMA complexes (Fig. S3).

Based on these results, we discuss the relationship between Fe(III)-DMA selectivity and structural differences in the loop region. As depicted in Fig. 2D, the chimera Zm-Hv-Zm showed lower Fe(II)-NA transport activity than did ZmYS1. This indicates that the activity of Zm-Hv-Zm, defined as k_{cat}/K_m, is lower than that of ZmYS1. In contrast, at high concentration (200 μM) of the NA complex, Hv-Zm-Hv, which showed a Fe(II)-NA transport activity similar to that of ZmYS1 (Fig. 2C,D), revealed the significantly higher activity than HvYS1, despite its high overall sequence identity (96%) with Hv-Zm-Hv. Furthermore, Hv-Zm-Hv had little selectivity for the Fe(III)-DMA or Fe(II)-NA complex at the high concentration. These results imply that the k_{cat} value of HvYS1 is not greatly dependent on the type of PS complex (DMA or NA), and thus, the transport efficiency (k_{cat}/K_m) of HvYS1 is mainly determined by the K_m value. As K_m is defined as $(k_{off} + k_{cat})/k_{on}$ (k_{on} and k_{off} are association and dissociation rate constants, respectively, upon binding of a PS complex to a transporter), an increase in the K_m value of HvYS1 for Fe(II)-NA should be caused by a decrease in the k_{on} value versus the k_{on} value for Fe(III)-DMA. This means that Fe(II)-NA binds HvYS1 more slowly than Fe(III)-DMA, supporting the hypothesis that the higher helical propensity of the loop region of HvYS1 has a greater preventative effect on the entrance of Fe(II)-NA than on that of Fe(III)-DMA (Fig. S3). Next, we asked why the helical propensity influences the binding of

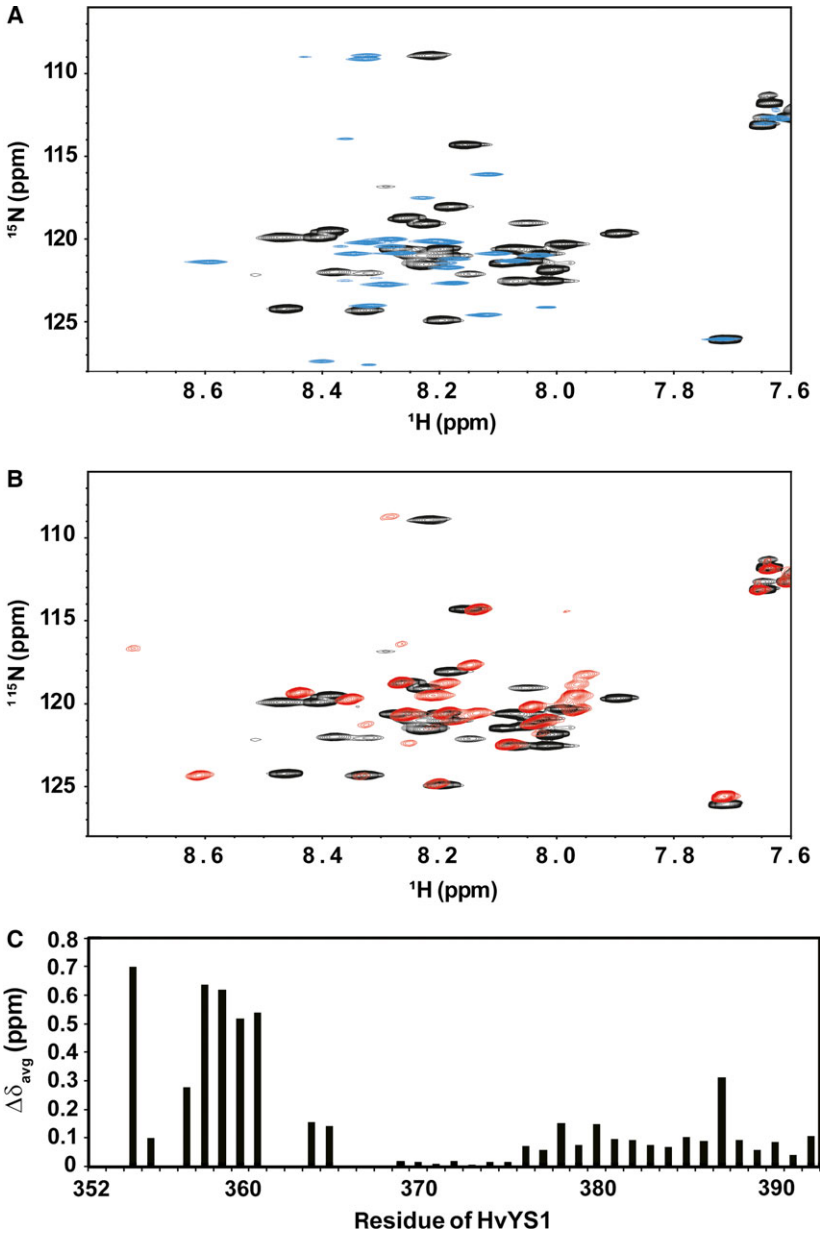

Fig. 4. Comparison of the ^{1}H-^{15}N HSQC spectra from the HvYS1 and ZmYS1 loop fragments in aqueous and membrane-mimicking solutions. (A) HSQC spectra of the HvYS1 (black) and ZmYS1 (blue) loop fragments in buffer. (B) HSQC spectra of the HvYS1 loop fragment in buffer without (black) and with (red) membrane-mimicking DPC micelles. (C) Weighted average chemical shift differences ($\Delta\delta_{avg}$) of amide ^{1}H and ^{15}N atoms between the HvYS1 loop fragment in the presence and absence of membrane-mimicking DPC micelles. $\Delta\delta_{avg}$ is calculated according using the equation $\Delta\delta_{avg} = \sqrt{\Delta\delta_{^{1}H}^{2} + (\Delta\delta_{^{15}N}/5)^{2}}$, where $\Delta\delta_{^{1}H}$ and $\Delta\delta_{^{15}N}$ are the chemical shift differences of ^{1}H and ^{15}N respectively.

the PS complexes. The loops possess both positively and negatively charged residues, which can be aligned in a helical structure. On the other hand, the charge distribution and hydration degree differ between Fe (III)-DMA and Fe(II)-NA. Therefore, both or either of these properties are likely important for the interaction between the PS complexes and the loops.

In this study, we focused on the differences in the loop structure between HvYS1 and ZmYS1, and we found that the E379, E380, H382 and Q384 residues in HvYS1 are responsible for forming a helical structure. These residues could possibly be involved in PS recognition, as charged residues are believed to participate in the recognition of trivalent and divalent metal-chelator substrate complexes [15]. YSL proteins belong to oligopeptide transporters (OPT), which are commonly found in bacteria, archaea, fungi and plants [45]. Recent studies have elucidated the crystal structures of several members of the proton-coupled oligopeptide transporter (POT) family of proteins [46–52]. Members of the POT family possess a conserved architecture, consisting of 14-transmembrane α-helices with N- and C-terminal helix bundles (H1–H6 and H7–H12) and two additional transmembrane α-helices (HA and HB). Thus, the predicted 14-transmembrane topology of YS1 transporters is in

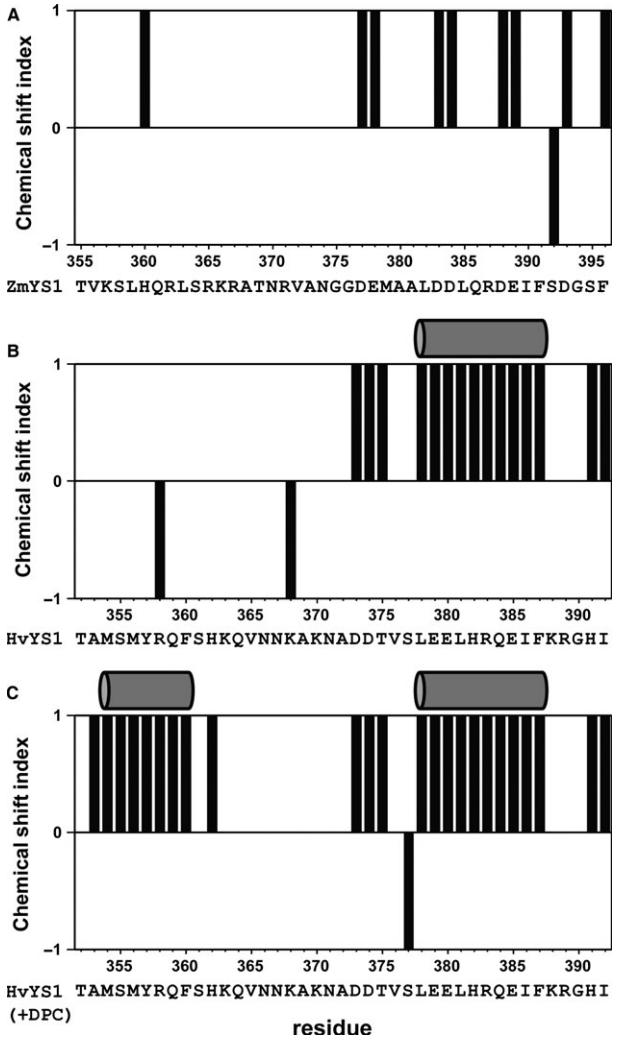

Fig. 5. Secondary structure predictions for the loop fragments obtained by chemical shift index (CSI) and the TALOS+ program. (A) ZmYS1 loop fragment in buffer, (B) HvYS1 loop fragment in buffer without membrane-mimicking DPC micelles and (C) with membrane-mimicking DPC micelles. Predicted helical structural regions are denoted by grey cylinders above CSI graph.

agreement with the OPT structures. Crystallization of plant YS1/YSL transporters has not been successful. Therefore, the structural features of the loop region shown in this study, which are expected to be responsible for substrate specificity, could facilitate future structure-based investigations into these transporters of plant origin.

Plant physiologists have attempted to produce alkaline-tolerant Poaceae plants by transformation with PS biosynthetic proteins and Fe(III)-PS transporters [53]. The level of tolerance to iron deficiency of barley is higher than that of rice because the amount of PS secreted in barley is significantly higher than that in rice. In addition, transgenic rice that biosynthesizes PS [54,55] and expresses *HvYS1* [56] has been shown to acquire alkaline tolerance. We have previously reported that the introduction of *HvYS1* into petunia (*Petunia hybrida*) grants the plant with significantly enhanced tolerance to alkaline hydroponic media in the presence of the Fe(III)-DMA complex [57]. In rice, an entire original transporter gene has been successfully replaced with the whole *HvYS1* gene [56]. Based on our data, we propose another strategy for modifying the substrate specificity of metal transporters by altering a small loop portion of the proteins, which could minimize the influence of these transporters on the fate and other functions of intrinsic proteins.

In conclusion, NMR and CD spectra of the loop fragments of HvYS1 and ZmYS1 transporters were determined along with the activities of HvYS1-ZmYS1 chimera transporters, and revealed that structural differences in the loop structure of the YS1/YSL transporter are associated with the substrate specificity of the transporter.

Acknowledgements

We thank Dr Elsbeth L. Walker for providing the *ZmYS1* cDNA and Dr Emiko Harada for preparing the expression vectors for oocytes and Drs Shigetada Nakanishi, Shoichi Kusumoto, Honoo Satake and Atsushi Yamagata for valuable discussions.

Author contributions

EH, KS, KN and YM designed and performed the experiments; EH and KS conducted the NMR and CD measurements; YM measured the transport activities; KN performed the synthesis experiments; and EH, KS and YM wrote the paper. All authors contributed to the discussion of the results. The authors declare that they have no competing interests.

References

1 Colangelo EP and Guerinot ML (2006) Put the metal to the petal: metal uptake and transport throughout plants. *Curr Opin Plant Biol* **9**, 322–330.
2 Briat JF, Curie C and Gaymard F (2007) Iron utilization and metabolism in plants. *Curr Opin Plant Biol* **10**, 276–282.
3 Römheld V and Marschner H (1986) Evidence for a specific uptake system for iron phytosiderophore in roots of grasses. *Plant Physiol* **80**, 175–180.

4 Mori S (1999) Iron acquisition by plants. *Curr Opin Plant Biol* **2**, 250–253.
5 Takagi S (1976) Naturally occurring iron-chelating compounds in oat- and rice-root washings. *Soil Sci Plant Nutr* **22**, 423–433.
6 Takemoto T, Nomoto K, Fushiya S, Ouchi R, Kusano G, Hikino H, Takagi S, Matuura Y and Kakudo M (1978) Structure of mugineic acid, a new amino acid possessing an iron-chelating activity from roots washing of water-cultured *Hordeum vulgare* L. *Proc Jpn Acad*, **54-B**, 469–473.
7 Ma JF, Kusano G, Kimura S and Nomoto K (1993) Specific recognition of mugineic acid-ferric complex by barley roots. *Phytochemistry* **34**, 599–603.
8 Curie C, Panaviene Z, Loulergue C, Dellaporta SL, Briat JF and Walker EL (2001) Maize yellow stripe1 encodes a membrane protein directly involved in Fe(III) uptake. *Nature* **409**, 346–349.
9 Araki R, Kousaka K, Namba K, Murata Y and Murata J (2015) 2′-Deoxymugineic acid promotes growth of rice (*Oryza sativa* L.) by orchestrating iron and nitrate uptake processes under high pH conditions. *Plant J* **81**, 233–246.
10 Yokosho K, Yamaji N, Ueno D, Mitani N and Ma JF (2009) OsFRDL1 is a citrate transporter required for efficient translocation of iron in rice. *Plant Physiol* **149**, 297–305.
11 Curie C, Cassin G, Couch D, Divol F, Higuchi K, Le Jean M, Misson J, Schikora A, Czernic P and Mari S (2009) Metal movement within the plant: contribution of nicotianamine and yellow stripe 1-like transporters. *Ann Bot* **103**, 1–11.
12 Schuler M, Rellán-Álvarez R, Fink-Straube C, Abadía J and Bauer P (2012) Nicotianamine functions in the phloem-based transport of iron to sink organs, in pollen development and pollen tube growth in *Arabidopsis*. *Plant Cell* **24**, 2380–2400.
13 Grillet L, Mari S and Schmidt W (2014) Iron in seeds – loading pathways and subcellular localization. *Front Plant Sci* **4**, 1–8.
14 Murata Y, Ma JF, Yamaji N, Ueno D, Nomoto K and Iwashita T (2006) A specific transporter for iron (III)-phytosiderophore in barley roots. *Plant J* **46**, 563–572.
15 Conte SS and Walker EL (2012) Genetic and biochemical approaches for studying the yellow stripe-like transporter family in plants. *Curr Top Membr* **69**, 295–322.
16 Roberts LA, Pierson AJ, Panaviene Z and Walker EL (2004) Yellow stripe1. Expanded roles for the maize iron-phytosiderophore transporter. *Plant Physiol* **135**, 112–120.
17 Schaaf G, Ludewig U, Erenoglu BE, Mori S, Kitahara T and von Wirén N (2004) ZmYS1 functions as a proton-coupled symporter for phytosiderophore- and nicotianamine-chelated metals. *J Biol Chem* **279**, 9091–9096.
18 Araki R, Murata J and Murata Y (2011) A novel barley yellow stripe 1-like transporter (HvYSL2) localized to the root endodermis transports metal-phytosiderophorecomplexes. *Plant Cell Physiol* **52**, 1931–1940.
19 Zheng L, Fujii M, Yamaji N, Sasaki A, Yamane M, Sakurai I, Sato K and Ma JF (2011) Isolation and characterization of a barley yellow stripe-like gene, HvYSL5. *Plant Cell Physiol* **52**, 765–774.
20 Inoue H, Kobayashi T, Nozoye T, Takahashi M, Kakei Y, Suzuki K, Nakazono M, Nakanishi H, Mori S and Nishizawa NK (2009) Rice OsYSL15 is an iron-regulated iron(III)-deoxymugineic acid transporter expressed in the roots and is essential for iron uptake in early growth of the seedlings. *J Biol Chem* **284**, 3470–3479.
21 Lee S, Chiecko JC, Kim SA, Walker EL, Lee Y, Guerinot ML and An G (2009) Disruption of OsYSL15 leads to iron inefficiency in rice plants. *Plant Physiol* **150**, 786–800.
22 Yordem BK, Conte SS, Ma JF, Yokosho K, Vasques KA, Gopalsamy SN and Walker EL (2011) *Brachypodium distachyon* as a new model system for understanding iron homeostasis in grasses: phylogenetic and expression analysis of Yellow Stripe-Like (YSL) transporters. *Ann Bot* **108**, 821–833.
23 Harada E, Sugase K, Namba K, Iwashita T and Murata Y (2007) Structural element responsible for the Fe(III)-phytosiderophore specific transport by HvYS1 transporter in barley. *FEBS Lett* **581**, 4298–4302.
24 Namba K, Murata Y, Horikawa M, Iwashita T and Kusumoto S (2007) A practical synthesis of the phytosderophore 2′-deoxymugineic acid: a key to the mechanistic study of iron acquisition by graminaceous plants. *Angew Chem Int Ed Engl* **46**, 7060–7063.
25 Sugase K, Landes MA, Wright PE and Martinez-Yamout M (2008) Overexpression of post-translationally modified peptides in *Escherichia coli* by co-expression with modifying enzymes. *Protein Expr Purif* **57**, 108–115.
26 Sreerama N and Woody RW (2000) Estimation of protein secondary structure from circular dichroism spectra: comparison of CONTIN, SELCON, and CDSSTR methods with an expanded reference set. *Anal Biochem* **287**, 252–260.
27 Sreerama N and Woody RW (2004) On the analysis of membrane protein circular dichroism spectra. *Protein Sci* **13**, 100–112.
28 Kay LE, Ikura M, Tschudin R and Bax A (1990) Three-dimensional triple resonance NMR spectroscopy of isotopically enriched proteins. *J Magn Reson* **89**, 496–514.

29 Grzesiek S and Bax A (1992) Improved 3D triple-resonance NMR techniques applied to a 31 kDa protein. *J Magn Reson* **96**, 432–440.
30 Grzesiek S and Bax A (1993) Amino acid type determination in the sequential assignment procedure of uniformly $^{13}C/^{15}N$-enriched proteins. *J Biomol NMR* **3**, 185–204.
31 Wittekind M and Mueller L (1993) HNCACB, a high-sensitivity 3D NMR experiment to correlate amide-proton and nitrogen resonances with the alpha-and beta-carbon resonances in proteins. *J Magn Reson, Ser B* **101**, 201–205.
32 Clubb RT, Thanabal V and Wagner G (1992) A new 3D HN(CA)HA experiment for obtaining fingerprint HN-Hα peaks in ^{15}N- and ^{13}C-labeled proteins. *J Biomol NMR* **2**, 203–210.
33 Grzesiek S, Anglister J and Bax A (1993) Correlation of backbone amide and aliphatic side-chain resonances in $^{13}C/^{15}N$-enriched proteins by isotropic mixing of ^{13}C magnetization. *J Magn Reson, Ser B* **101**, 114–119.
34 Salzmann M, Wider G, Pervushin K, Senn H and Wüthrich K (1999) TROSY-type triple-resonance experiments for sequential NMR assignments of large proteins. *J Am Chem Soc* **121**, 844–848.
35 Delaglio F, Grzesiek S, Vuister GW, Zhu G, Pfeifer J and Bax A (1995) NMRPipe: a multidimensional spectral processing system based on UNIX pipes. *J Biomol NMR* **6**, 277–293.
36 Kobayashi N, Iwahara J, Koshiba S, Tomizawa T, Tochio N, Güntert P, Kigawa T and Yokoyama S (2007) KUJIRA, a package of integrated modules for systematic and interactive analysis of NMR data directed to high-throughput NMR structure studies. *J Biomol NMR* **39**, 31–52.
37 Kobayashi N, Harano Y, Tochio N, Nakatani E, Kigawa T, Yokoyama S, Mading S, Ulrich EL, Markley JL, Akutsu H *et al.* (2012) An automated system designed for large scale NMR data deposition and annotation: application to over 600 assigned chemical shift data entries to the BioMagResBank from the Riken Structural Genomics/Proteomics Initiative internal database. *J Biomol NMR* **53**, 311–320.
38 Shen Y, Delaglio F, Cornilescu G and Bax A (2009) TALOS+: a hybrid method for predicting protein backbone torsion angles from NMR chemical shifts. *J Biomol NMR* **44**, 213–223.
39 Hirokawa T, Boon-Chieng S and Mitaku S (1998) SOSUI: classification and secondary structure prediction system for membrane proteins. *Bioinformatics* **14**, 378–379.
40 Tsirigos KD, Peters C, Shu N, Käll L and Elofsson A (2015) The TOPCONS web server for combined membrane protein topology and signal peptide prediction. *Nucleic Acids Res* **43**, W401–W407.
41 Krogh A, Larsson B, von Heijne G and Sonnhammer LLE (2001) Predicting transmembrane protein topology with a hidden Markov model: application to complete genomes. *J Mol Biol* **305**, 567–580.
42 Zhang L, DeHaven RN and Goodman M (2002) NMR and modeling studies of a synthetic extracellular loop II of the κ opioid receptor in a DPC micelle. *Biochemistry* **41**, 61–68.
43 Wittlich M, Koenig BW, Stoldt M, Schmidt H and Willbold D (2009) NMR structural characterization of HIV-1 virus protein U cytoplasmic domain in the presence of dodecylphosphatidylcholine micelles. *FEBS J* **276**, 6560–6575.
44 Singarapu KK, Tonelli M, Chow DC, Frederick RO, Westler WM and Markley JL (2011) Structural characterization of Hsp12, the heat shock protein from *Saccharomyces cerevisiae*, in aqueous solution where it is intrinsically disordered and in detergent micelles where it is locally α-helical. *J Biol Chem* **286**, 43447–43453.
45 Yen MR, Tseng YH and Saier MH Jr (2001) Maize yellow stripe 1, an iron-phytosiderophore uptake transporter, is a member of the oligopeptide transporter (OPT) family. *Microbiology* **147**, 2881–2883.
46 Newstead S, Drew D, Cameron AD, Postis VL, Xia X, Fowler PW, Ingram JC, Carpenter EP, Sansom MS, McPherson MJ *et al.* (2011) Crystal structure of a prokaryotic homologue of the mammalian oligopeptide-proton symporters, PepT1 and PepT2. *EMBO J* **30**, 417–426.
47 Solcan N, Kwok J, Fowler PW, Cameron AD, Drew D, Iwata S and Newstead S (2012) Alternating access mechanism in the POT family of oligopeptide transporters. *EMBO J* **31**, 3411–3421.
48 Doki S, Kato HE, Solcan N, Iwaki M, Koyama M, Hattori M, Iwase N, Tsukazaki T, Sugita Y, Kandori H *et al.* (2013) Structural basis for dynamic mechanism of proton-coupled symport by the peptide transporter POT. *Proc Natl Acad Sci USA* **110**, 11343–11348.
49 Guettou F, Quistgaard EM, Trésaugues L, Moberg P, Jegerschöld C, Zhu L, Jong AJO, Nordlund P and Löw C (2013) Structural insights into substrate recognition in proton-dependent oligopeptide transporters. *EMBO Rep* **14**, 804–810.
50 Lyons JA, Parker JL, Solcan N, Brinth A, Li D, Shah ST, Caffrey M and Newstead S (2014) Structural basis for polyspecificity in the POT family of proton-coupled oligopeptide transporters. *EMBO Rep* **15**, 886–893.
51 Guettou F, Quistgaard EM, Raba M, Moberg P, Löw C and Nordlund P (2014) Selectivity mechanism of a bacterial homolog of the human drug-peptide transporters PepT1 and PepT2. *Nat Struct Mol Biol* **21**, 728–731.
52 Fowler PW, Orwick-Rydmark M, Radestock S, Solcan N, Dijkman PM, Lyons JA, Kwok J, Caffrey M, Watts A, Forrest LR *et al.* (2015) Gating topology of the

proton-coupled oligopeptide symporters. *Structure* **23**, 290–301.
53 Schroeder JI, Delhaize E, Frommer WB, Guerinot ML, Harrison MJ, Herrera-Estrella L, Horie T, Kochian LV, Munns R, Nishizawa NK *et al.* (2013) Using membrane transporters to improve crops for sustainable food production. *Nature* **497**, 60–66.
54 Masuda H, Aung MS and Nishizawa NK (2013) Iron biofortification of rice using different transgenic approaches. *Rice (NY)* **6**, 40.
55 Lee S, Jeon US, Lee SJ, Kim YK, Persson DP, Husted S, Schjørring JK, Kakei Y, Masuda H, Nishizawa NK *et al.* (2009) Iron fortification of rice seeds through activation of the nicotianamine synthase gene. *Proc Natl Acad Sci USA* **106**, 22014–22019.
56 Gómez-Galera S, Sudhakar D, Pelacho AM, Capell T and Christou P (2012) Constitutive expression of a barley Fe phytosiderophore transporter increases alkaline soil tolerance and results in iron partitioning between vegetative and storage tissues under stress. *Plant Physiol Biochem* **53**, 46–53.
57 Murata Y, Itoh Y, Iwashita T and Namba K (2015) Transgenic petunia with the iron (III)-phytosiderophore transporter gene acquires tolerance to iron deficiency in alkaline environments. *PLoS One* **10**, e0120227.

Supporting information

Additional Supporting Information may be found online in the supporting information tab for this article:

Fig. S1. Protein sequence alignment of YS1/YSL family transporters.

Fig. S2. Transport activities of HvYS1, ZmYS1 and the chimeras.

Fig. S3. Schematic illustration of the Fe(III)-DMA selectivity of HvYS1 as compared with ZmYS1 based on the helix propensity of an extracellular loop.

Table S1. Transmembrane topology predictions of YS1/YSL transporters and helical propensity predictions of the loop of the transporters.